International Journal of Advance Research in Science and Engineering
Vol. No.5, Issue No. 10 , October 2016
www.ijarse.com
IJARSE
ISSN (O) 2319 - 8354
ISSN (P) 2319 - 8346

DUFOUR AND SORET EFFECTS ON UNSTEADY MIXED CONVECTION FLOW OVER EXPONENTIALLY PERMEABLE STRETCHING SURFACE WITH DARCY-FORCHHIEMER POROUS MEDIUM

P. M. Patil[1], Nafisa A. Kumbarwadi[2], S. Roy[3], Ebrahim Momoniat[4]

[1,2]Department of Mathematics, KarnatakUniversity,
Pawate Nagar, Dharwad, Karnataka, (India)
[3]Department of Mathematics, I. I. T Madras, Chennai
[4]DST/NRF Centre of Excellence in the Mathematical and Statistical Sciences, School of Computer Science and Applied Mathematics, University of Witwatersrand, Private Bag-3, Wits-2050, Johannesburg, South Africa

ABSTRACT

In this article, we study unsteady mixed convection flow over exponentially stretching permeable vertical surface in presence of soret, dufour and Darcy-Forchheimer porous medium. The set of governing nonlinear coupled partial differential equations are transformed to system of dimensionless nonlinear partial differential equations by using appropriate non-similar transformations. The Quasi-linearization technique in conjunction with implicit finite difference scheme is used to solve the set of non-dimensional partial differential equations. The effects of various governing parameters like dufour, soret,Schmidt number, mixed convection parameter and permeability on flow, species concentration, temperature, heat transfer, mass transfer, skin friction coefficients are discussed and displayed graphically.

Keywords: Exponentially Permeable Stretching Surface, Unsteady Mixed Convection, Non-Similar Solution, Darcy-Forchheimer Porous Medium, Soret And Dufour Effects.

I. INTRODUCTION

The diffusion of mass due to varying temperature is known as Soret effect and diffusion of heat caused by varying concentration is termed as Dufour effect. These effects are significant when the density differences arise in the fluid flow. The cross diffusion have wide range of applications in the study of petrology, hydrology and geosciences, etc. Soret effect has many applications as name few, refinement of crude oil, transport mechanism in fouling, crystal growth in microgravity, manufacturing of optical fiber in vacuum deposition processes, etc. Kefayati [1] investigated the effects of Soret and Dufour on double-diffusive natural convection of power law fluids in an inclined porous cavity. Shrinivacharya *et al.* [2] examined steady mixed convection flow through

IJARSE
ISSN (O) 2319 - 8354
ISSN (P) 2319 - 8346

wavy surface with Dufour and Soret effects and variable thermal conductivity, viscosity in a porous medium. Very recently, Patil*et al*. [3] examined mixed convection flows over an exponentially impermeable stretching surface with thermal diffusion and diffusion-thermo effects.

The flow through porous medium has attracted considerable attention of many researchers/investigators due to their widespread practical applications in petroleum reservoirs, geothermal processes, thermal insulation, food processing, chemical catalytic reactors, heat exchangers, etc. Generally, Darcy law states that the pressure gradient is linearly proportional to velocity, is only suitable for laminar flow with small porosity and low velocity. But in many practical situations the Darcy law is not applicable, such as in case of fluid flow with high velocity, porous medium bounded by impermeable wall, high porosity near the wall region. Thus, it is essential to incorporate the inertia effect or non-Darcian term, which is used to describe high velocity flow and nonlinear porosity. Hence, we added the velocity squared term to momentum equation which is known as inertia term or Forchhiemer drag parameter. Chen and Chen [4] studied the non-Darcian flow effects on mixed convection flows in a saturated porous medium near a vertical surface. Effect of variable viscosity on MHD non-Darcy mixed convection heat transfer from a stretching sheet embedded in a porous medium with non-uniform heat source/sink examined by Pal and Mondal [5].

The suction/injection processes has many practical applications in science and engineering, such as drying, cooling of tower design, thermal oil recovery,to remove reactants, radial diffuser, etc. Generally, suction enhances the heat transfer, skin friction and mass transfer coefficient where injection acts in opposite manner. Suction/injection effects on thermophoresis particle deposition in a non-Darcy porous medium under the influence of Soret, Dufour effects studied by Partha[6]. Chamkha*et al*. [7] have investigated similarity solution for unsteady heat and mass transfer over a stretching surface embedded in a porous medium with suction/injection and chemical reaction effects. Mukhopadhyay[8] has studied slip effects on MHD boundary layer flow over an exponentially stretching sheet with suction/blowing and thermal radiation. Non-uniform mass transfer with heat absorption or generation and chemical reaction of unsteady flow through stretching sheet investigated by Ravindran and Samyuktha[9].

Heat and mass transfer analysis for fluid flow over an exponentially stretching porous sheet with surface heat flux in porous medium investigated by Mandal and Mukhopadhyay [10]. Sharada and Bhandari [11] studied heat and mass transfer of a Casson fluid over an vertical exponentially stretching surface by considering the effect of thermal radiation, Soret and Dufour, chemical reaction. The flow through exponentially stretching sheet has various applications in science and technology, such as in thinning and annealing of copper wires, etc. A large number of researchers restricted(confined) their studies to either unsteady similar flows or steady non-similar flows, because of the mathematical complexity in analysing the non-similar solutions of unsteady flows. The effects of variable concentration and temperature on mixed convection flow through stretching sheet with surface mass transfer discussed by Patil *et al.* [12]. Patil *et al.* [13] have investigated unsteady mass and heat transfer with variable temperature and concentration over stretching sheet in a parallel free stream.

To the best of author's knowledge the cross diffusion over exponentially stretching of unsteady mixed convection flow with suction/injection, Darcy-Forchhiemer porous medium is not reported earlier. Thus, we are interested to get non-similar solution of unsteady double diffusive mixed convection flow with cross diffusion, suction/injection, and porous medium along exponentially stretching surface. The boundary layer equations are

IJARSE
ISSN (O) 2319 - 8354
ISSN (P) 2319 - 8346

transformed to non-dimensional equations using non-similar transformations. Finally, we have used implicit finite difference scheme in combination with Quasi-linearization technique [14] to solve resulting set of dimensionless partial differential equations and results are compared and validated with earlier published data.

II. ANALYSIS

Consider an unsteady double diffusive mixed convection boundary layer flow bounded by a semi-infinite permeable vertical exponentially stretching sheet with Dufour, Soret effects and Darcy-Forchheimer porous medium. The x-axis is taken along the plate in the vertically upward direction and the y-axis is taken normal to it. Figure 1 shows the schematic representation of the physical model and coordinate system. We assume that, all thermo-physical properties of the fluid are constant except density variations causing the body force, concentration and temperature variations causing the buoyancy forces in the momentum equations. Boussinesq approximation (Schlichting and Gersten[15])is used to couple the temperature and species concentration fields to the flow field. Under these considerations, the equations of conservation of mass, momentum, temperature and species concentration governing flow are given by [16]

$$\frac{\partial u}{\partial x}+\frac{\partial v}{\partial y}=0, \tag{1}$$

$$\frac{\partial u}{\partial t}+u\frac{\partial u}{\partial x}+v\frac{\partial u}{\partial y}=\frac{\partial U_e}{\partial t}+U_e\frac{dU_e}{dx}+\nu\frac{\partial^2 u}{\partial y^2}+g\left[\beta\left(T-T_\infty\right)+\beta^*\left(C-C_\infty\right)\right] -\frac{\varepsilon\nu}{K}\left(u-U_e\right)-\frac{S\varepsilon^2}{K^{1/2}}\left(u^2-U_e^2\right), \tag{2}$$

$$\frac{\partial T}{\partial t}+u\frac{\partial T}{\partial x}+v\frac{\partial T}{\partial y}=\frac{\nu}{\Pr}\frac{\partial^2 T}{\partial y^2}+\frac{D_m k_T}{C_s C_p}\frac{\partial^2 C}{\partial y^2}, \tag{3}$$

$$\frac{\partial C}{\partial t}+u\frac{\partial C}{\partial x}+v\frac{\partial C}{\partial y}=\frac{\nu}{Sc}\frac{\partial^2 C}{\partial y^2}+\frac{D_m k_T}{T_m}\frac{\partial^2 T}{\partial y^2}, \tag{4}$$

The physical boundary conditions are given by

$$y=0: u=U_W(x,t), v=v_w, T=T_W=T_\infty+(T_{W0}-T_\infty)\exp\left(\frac{2x}{L}\right),$$

$$C=C_W=C_\infty+(C_{W0}-C_\infty)\exp\left(\frac{2x}{L}\right),$$

$$y\to\infty: u\to U_e\left(x,t\right), \quad T\to T_\infty, \quad C\to C_\infty. \tag{5}$$

The wall stretching sheet velocity $U_w\left(x\right)$ and free stream velocity $U_e\left(x\right)$ are respectively defined by $U_W(x,t)=U_0\phi\left(\tau\right)\exp\left(\frac{x}{L}\right), U_e(x,t)=U_\infty\phi\left(\tau\right)\exp\left(\frac{x}{L}\right)$, where U_0 is the reference velocity; L is the characteristic length and U_∞ is the free stream velocity.

International Journal of Advance Research in Science and Engineering
Vol. No.5, Issue No. 10 , October 2016
www.ijarse.com
IJARSE
ISSN (O) 2319 - 8354
ISSN (P) 2319 - 8346

Applying the following transformations:

$$\left.\begin{aligned}
&\xi = \frac{x}{L}, \eta = \left(\frac{U_0}{\nu x}\right)^{1/2} \exp\left(\frac{x}{2L}\right) y, \tau = \frac{U_0^2 \exp\left(\frac{x}{L}\right)}{\nu} t, \\
&\psi(x,y,t) = (\nu U_0 x)^{1/2} \exp\left(\frac{x}{2L}\right) \phi(\tau) f(\xi,\eta,\tau), \\
&T - T_\infty = (T_w - T_\infty) G(\xi,\eta,\tau),\ (T_W - T_\infty) = (T_{W0} - T_\infty) \exp\left(\frac{2x}{L}\right), \\
&C - C_\infty = (C_w - C_\infty) H(\xi,\eta,\tau),\ (C_W - C_\infty) = (C_{W0} - C_\infty) \exp\left(\frac{2x}{L}\right), \\
&u = \frac{\partial \psi}{\partial y},\ v = -\frac{\partial \psi}{\partial x},\ u = U_0 \phi(\tau) \exp\left(\frac{x}{L}\right) F, \\
&v = -\frac{1}{2}\left(\frac{\nu U_0}{x}\right)^{1/2} \phi(\tau) \exp\left(\frac{x}{2L}\right) \left\{(1+\xi) f + 2\xi f_\xi + \eta(\xi - 1) F + \tau\xi(f_\tau + \phi_\tau \phi^{-1} f)\right\},
\end{aligned}\right\} \quad (6)$$

toEqs. (1) - (4), we find that Eq. (1) is trivially satisfied, and Eqs. (2) - (4) reduce to

$$F_{\eta\eta} + \phi(\tau)[(1+\xi)\frac{f}{2} + \xi\tau(f_\tau + \phi_\tau \phi^{-1}(\tau) f)] F_\eta - \phi \xi F^2 - \phi(\tau)\left\{\xi\tau(F_\tau + \phi_\tau \phi^{-1}(\tau) F)\right\} F$$

$$-\xi \operatorname{Re} \phi^{-1}(\tau) \phi_\tau F - \operatorname{Re} \xi F_\tau + \xi \operatorname{Re} \phi^{-1}(\tau) \phi_\tau \beta + \beta^2 \xi(\phi(\tau) + \tau \phi_\tau) + Ri \xi \phi^{-1}(\tau)(g + N h)$$

$$-\frac{\xi e^{-\xi}}{Da \operatorname{Re}}(F - \beta) - \xi \phi(\tau) \Gamma\left(F^2 - \beta^2\right) = \xi \phi(\tau)\left\{F F_\xi - f_\xi F_\eta\right\}, \quad (7)$$

$$G_{\eta\eta} + \Pr \phi(\tau)\left\{(1+\xi)\frac{f}{2} + \tau\xi(f_\tau + \phi^{-1}(\tau)\phi_\tau f)\right\} G_\eta - 2\phi(\tau) \Pr \xi F G - \xi \Pr(\operatorname{Re} + \phi(\tau)\tau F) G_\tau$$

$$+ \Pr D_f H_{\eta\eta} = \Pr \xi \phi(\tau)\left\{F G_\xi - f_\xi G_\eta\right\}, \quad (8)$$

$$H_{\eta\eta} + Sc\,\phi(\tau)\left\{(1+\xi)\frac{f}{2} + \xi\tau(f_\tau + \phi^{-1}(\tau)\phi_\tau f)\right\} H_\eta - 2 Sc \xi \phi(\tau) F H - \xi Sc(\operatorname{Re} + \phi(\tau)\tau F) H_\tau$$

$$+ Sc\,Sr\,G_{\eta\eta} = Sc \xi \phi(\tau)\left\{F H_\xi - f_\xi H_\eta\right\}. \quad (9)$$

The non-dimensional boundary conditions (5) become

International Journal of Advance Research in Science and Engineering
Vol. No.5, Issue No. 10 , October 2016
www.ijarse.com
IJARSE
ISSN (O) 2319 - 8354
ISSN (P) 2319 - 8346

$$\eta = 0 \ : \quad F = 1, \quad G = 1, \quad H = 1,$$
$$\eta \to \infty : \quad F \to \beta, \quad G \to 0, \quad H \to 0, \qquad (10)$$

Here $f(\xi,\eta) = \int_0^{\eta} F\, d\eta + f_W$ and f_W can be obtained from transformations as,

$$v = -\frac{1}{2}\left(\frac{\nu U_0}{x}\right)^{1/2} \phi(\tau) \exp\left(\frac{x}{2L}\right)\left\{(1+\xi) f + 2\xi f_{\xi} + \eta(\xi - 1)F + \tau\xi(f_{\tau} + \phi_{\tau}\phi^{-1} f)\right\}$$

In view of boundary condition (5) and $v_w = v_0 \exp\left(\frac{x}{2L}\right)$, we get

$$v_0 \exp\left(\frac{x}{2L}\right) = -\frac{1}{2}\left(\frac{\nu U_0}{x}\right)^{1/2} \phi(\tau) \exp\left(\frac{x}{2L}\right)\left\{(1+\xi) f + 2\xi f_{\xi} + \eta(\xi - 1)F + \tau\xi(f_{\tau} + \phi_{\tau}\phi^{-1} f)\right\}$$

$$i.e., \left\{(1+\xi) f_W + 2\xi (f_{\xi})_W + \tau\xi((f_{\tau})_w + \phi_{\tau W}\phi^{-1} f_w)\right\} = -\frac{\xi^{1/2} 2v_0}{\phi(\tau)}\left(\frac{L}{\nu U_0}\right)^{1/2} = A\frac{\xi^{1/2}}{\phi(\tau)}$$

Where $A = -2v_0\left(\frac{L}{\nu U_0}\right)^{1/2} = \text{constant}$, is the surface mass transfer parameter with $A > 0$ for the suction, $A < 0$ for the injection or blowing and $A = 0$ for an impermeable surface. Using the characteristic length L, the dimensional variable x is changed into non-dimensional variable ξ.

The momentum Eq. (7), the energy Eq. (8) and the species concentration Eq. (9) are coupled with each other. Furthermore, the Richardson number *Ri*, which characterizes the mixed convection effects, N is the ratio between the solutal buoyancy and the thermal forces, *Da* is Darcy number, β is the velocity ratio parameter, Γ is Forchheimer drag coefficient, Df is the Dufour number and Sr is the Soret number and they are defined, respectively, as

$$Ri = \frac{Gr}{\mathrm{Re}^2},\ N = \frac{Gr^*}{Gr},\ Da = \frac{K}{\varepsilon L^2},\ \beta = \frac{U_{\infty}}{U_0},\ \Gamma = \frac{S\varepsilon^2}{K^{1/2}},\ Df = \frac{D_m k_T}{\nu C_s C_p}\left(\frac{C_w - C_{\infty}}{T_w - T_{\infty}}\right)$$

and $Sr = \frac{D_m k_T}{\nu T_m}\left(\frac{T_w - T_{\infty}}{C_w - C_{\infty}}\right)$, (11)

where Grashof number, $Gr = g\beta(T_{w0} - T_{\infty})L^3/\nu^2$ mentioning to the wall temperature, $Gr^* = g\beta^*(C_{w0} - C_{\infty})L^3/\nu^2$ is the Grashof number mentioning to the wall species concentration and

IJARSE
ISSN (O) 2319 - 8354
ISSN (P) 2319 - 8346

$\mathrm{Re}=U_0 L/\nu$ is the Reynolds number. The flow is steady at $\tau = \mathrm{O}$ and becomes unsteady $\tau > \mathrm{O}$ because of exponentially stretching wall velocity varies with time, and this wall velocity given by $U_w(x)=U_0\,\phi(\tau)\exp\left(\frac{x}{L}\right)$ and free stream velocity $U_e(x)=U_\infty\,\phi(\tau)\exp\left(\frac{x}{L}\right)$, where $\phi(\tau)=1+\alpha\tau^2$.

Thus, the initial conditions (*i .e.* conditions at $\tau=0$) are given by the steady state equations obtained from (7) - (9) by substituting $F_\tau=d\phi/d\tau=G_\tau=H_\tau=0$, $\phi(\tau)=1$ when $\tau=0$ [12, 13].

The physical quantities of practical interest are given by the Nusselt number Nu, C_f the skin friction coefficient and the Sherwood number Sh, which signify the heat transfer rate, the shear stress, the mass transfer rate at the surface, respectively. These coefficients are defined, respectively, as

$$C_f=\mu\frac{2(\partial u/\partial y)_{y=0}}{\rho U_w{}^2}=2\,\mathrm{Re}^{-1/2}\,\xi^{-1/2}\exp(\xi)^{-1/2}\,\phi^{-1}\,F_\eta(\xi,0),$$

$$i.e.,\ \left(\mathrm{Re}\,\xi\exp(\xi)\right)^{1/2}C_f=2\phi^{-1}F_\eta(\xi,0). \tag{12}$$

$$Nu=-x\frac{(\partial T/\partial y)_{y=0}}{(T_w-T_\infty)}=-\left(\mathrm{Re}\,\xi\exp(\xi)\right)^{1/2}G_\eta(\xi,0),$$

$$i.\,e.,\ \left(\mathrm{Re}\,\xi\exp(\xi)\right)^{-1/2}Nu=-G_\eta(\xi,0). \tag{13}$$

$$Sh=-x\frac{(\partial C/\partial y)_{y=0}}{(C_w-C_\infty)}=-\left(\mathrm{Re}\,\xi\exp(\xi)\right)^{1/2}H_\eta(\xi,0),$$

$$i.e.,\ \left(\mathrm{Re}\,\xi\exp(\xi)\right)^{-1/2}Sh=-H_\eta(\xi,0). \tag{14}$$

III. METHOD OF SOLUTION

The numerical method used for this investigation is the implicit finite difference scheme in conjunction with Quasi-linearization technique [14]. A central difference formula is applied across the boundary layer direction *i. e.*, η - direction and backward difference formula in streamwise ξ and time τ directions. By employing, the Quasi-linearization technique [14], the non-dimensional non-linear partial differential equations are transformed to iterative linear partial differential equations. The application of this technique has the quadratic rate of convergence.

$$F_{\eta\eta}^{i+1}+A_1^i\,F_\eta^{i+1}+A_2^i\,F^{i+1}+A_3^i\,F_\xi^{i+1}+A_4^i\,F_\tau^{i+1}+A_5^i\,G^{i+1}+A_6^i\,H^{i+1}=A_7^i, \tag{15}$$

$$G_{\eta\eta}^{i+1}+B_1^i\,G_\eta^{i+1}+B_2^i\,G^{i+1}+B_3^i\,G_\xi^{i+1}+B_4^i\,G_\tau^{i+1}+B_5^i\,F_\eta^{i+1}+B_6^i\,H_{\eta\eta}^{i+1}=B_7^i, \tag{16}$$

$$H_{\eta\eta}^{i+1}+C_1^i\,H_\eta^{i+1}+C_2^i\,H^{i+1}+C_3^i\,H_\xi^{i+1}+C_4^i\,H_\tau^{i+1}+C_5^i\,F^{i+1}+C_6^i\,G_{\eta\eta}^{iA+1}=C_7^i. \tag{17}$$

The coefficient functions with iterative index *i* are known and the functions with iterative index (*i*+1) are to be determined. The corresponding boundary conditions are given by

IJARSE
ISSN (O) 2319 - 8354
ISSN (P) 2319 - 8346

$$F^{i+1}(\xi,0)=1,\quad G^{i+1}(\xi,0)=1,\quad H^{i+1}(\xi,0)=1 \quad \text{at } \eta=0,$$
$$F^{i+1}(\xi,\eta)=\beta,\ G^{i+1}(\xi,\eta)=0,\ H^{i+1}(\xi,\eta)=0 \quad \text{at} \quad \eta=\eta_\infty. \qquad (18)$$

The coefficients in equation (15) - (17) are given by

$$A_1^i=\phi\{(1+\xi)\frac{f}{2}+\xi f_\xi+\xi\tau(f_\tau+\phi^{-1}\phi_\tau f)\};$$

$$A_2^i=-\xi\phi\left(2F+F_\xi+\tau F_\tau+2\phi^{-1}\phi_\tau\tau F\right)-\mathrm{Re}\,\xi\,\phi^{-1}\phi_\tau-\frac{\xi e^{\xi}}{Da\,\mathrm{Re}}-2\Gamma\xi\phi F;\ A_3^i=-\xi\phi F;$$

$$A_4^i=-\xi(\phi\tau F+\mathrm{Re});\ A_5^i=\phi^{-1}\xi Ri;\ A_6^i=\phi^{-1}\xi RiN;$$

$$A_7^i=-\xi\phi F(F+F_\xi+\tau F_\tau)-\xi\tau\phi_\tau F^2-\beta\xi(\mathrm{Re}\phi^{-1}\phi_\tau+\beta\phi+\beta\tau\phi_\tau)-\xi\phi\Gamma F^2-\xi\phi\Gamma\beta^2-\frac{\xi e^{\xi}}{Da\,\mathrm{Re}}\beta;$$

$$B_1^i=\mathrm{Pr}\,\phi\{(1+\xi)\frac{f}{2}+\xi\tau(f_\tau+\phi^{-1}\phi_\tau f)+\xi f_\xi\};$$

$$B_2^i=-2\,\mathrm{Pr}\,\phi\xi F;$$

$$B_3^i=-\mathrm{Pr}\,\phi\xi F;$$

$$B_4^i=-\xi\,\mathrm{Pr}(\mathrm{Re}+\phi\tau F);$$

$$B_5^i=-\mathrm{Pr}\,\phi\,\xi(2G+\tau G_\tau+G_\xi);$$

$$B_6^i=\mathrm{Pr}\,Df;$$

$$B_7^i=-\mathrm{Pr}\,\phi\xi F(2G+\tau G_\tau+G_\xi);$$

$$C_1^i=Sc\,\phi\{(1+\xi)\frac{f}{2}+\xi\tau(f_\tau+\phi^{-1}\phi_\tau f)+\xi f_\xi\};$$

$$C_2^i=-2\,Sc\,\xi\phi F;$$

$$C_3^i=-Sc\,\xi\phi F;$$

$$C_4^i=-Sc\,\xi(\mathrm{Re}+\phi\tau F);$$

$$C_5^i=-Sc\,\xi\phi(\tau H_\tau+H_\xi+2H);$$

$$C_6^i=Sc\,Sr;$$

$$C_7^i=-Sc\,\xi\phi F(\tau H_\tau+H_\xi+2H).$$

The final equations can be put into a sequence of linear algebraic equations with a block tri-diagonal matrix, further it can be solved by Varga's algorithm [17]. We have chosen step sizes of $\Delta\eta$, $\Delta\xi$ and $\Delta\tau$ as 0.01, 0.01 and 0.01, respectively. The numerical solution is converged and the iteration process is terminated when the difference reaches less than 10^{-5}, *i. e.*,

International Journal of Advance Research in Science and Engineering
Vol. No.5, Issue No. 10 , October 2016
www.ijarse.com
IJARSE
ISSN (O) 2319 - 8354
ISSN (P) 2319 - 8346

$$\text{Max}\left\{\left|\left(F_\eta\right)_w^{i+1}-\left(F_\eta\right)_w^{i}\right|,\left|\left(G_\eta\right)_w^{i+1}-\left(G_\eta\right)_w^{i}\right|,\left|\left(H_\eta\right)_w^{i+1}-\left(H_\eta\right)_w^{i}\right|\right\}<10^{-5}. \qquad (19)$$

The present numerical results are compared with Patil *et al.* [12], Patil *et al.* [13], and Ravindran and Samyuktha[9] to validate the accuracy and convergence. The present results are found to be in good agreement with earlier published data as given in **Table 1**.

In support of non-similar solutions the effects of all the physical parameters involved in the problem, some of the numerical results pertaining to skin friction parameter $\left(\text{Re}\right)^{1/2} C_f$, heat transfer parameter $\left(\text{Re}\right)^{-1/2} Nu$ and mass transfer parameter $\left(\text{Re}\right)^{-1/2} Sh$ are tabulated in **Table 2**.

IV. RESULTS AND DISCUSSION

The system of dimensionless equations (7) - (9) with the boundary conditions (10) have been solved numerically by using Quasi-linearization technique [14] with implicit finite difference scheme [12, 13]. The numerical procedure have been carried out for different values of Ri $(-1 \le Ri \le 3)$, β $(0.5 \le \beta \le 1.5)$, α $(-0.2 \le \alpha \le 0.2)$, τ $(0 \le \tau \le 1)$, N $(-1 \le N \le 3)$, Df $(0.1 \le Df \le 1.5)$, $\text{Pr}(0.7 \le \text{Pr} \le 7.0)$, $Sc(0.66 \le Sc \le 2.57)$, $Sr(0.1 \le Sr \le 1.5)$, Γ $(0.0 \le \Gamma \le 2.0)$, $Da(1.0 \le Da \le 1000000)$. The edge of the boundary layer η_∞ has been considered between 4.0 and 12.0 depending on the values of the governing parameters. The numerical solutions have been obtained for both accelerating $[\phi(\tau) = 1 + \alpha\tau^2; \alpha > 0, 0 \le \tau \le 1]$ and decelerating $[\phi(\tau) = 1 + \alpha\tau^2; \alpha < 0, 0 \le \tau \le 1]$ free stream velocities of the fluid. It may be noted that the range of parameter values is used for air and water at different temperatures. For example, *Pr* = 0.7 for air, *Pr* = 7.0 for water at $20^0 C$ and the value of *Pr* reduces for water at higher temperature.

Figure 2 depict the effects of streamwise coordinate ξ and time variable τ on the temperature and velocity profile $G(\xi,\eta,\tau)), (F(\xi,\eta,\tau)$ for accelerating flow $\phi(\tau) = 1 + \alpha\tau^2$, $\alpha = 1$ when β=0.5, N=1.0, Γ=1.0, Re= 2.0, Ri=1.0, Df =0.5, Pr=0.7, Sr=0.5, Sc=0.94, Da=1.0 and A=1.0. The temperature and velocity profiles are decreasing with the increase of streamwise coordinate ξ and time τ from 0 to 1. The physical reason is that an increase in the streamwise coordinate ξ acts as an adverse pressure gradient in the velocity and temperature profile, which reduces the magnitude of the both profiles. Thus, fluid flows with reduced velocity. Also, it is well known that the presence of the porous medium in the flow creates an obstacle to fluid flow causing the flow to move slower and enhances the temperature. Because of the porous medium and suction the velocity and momentum boundary layer thickness decreases. In particular, for

Example, $\alpha = 1,\ \text{Re} = 2,\ \beta = 0.5,\ Ri = 1,\ \text{Pr} = 0.7,$ $Df = 0.5, Sr = 0.5, \Gamma = 0.5, N = 1, A = 1, Da = 1,$ the velocity profile decreases by 11% as ξ increases

IJARSE
ISSN (O) 2319 - 8354
ISSN (P) 2319 - 8346

from $\xi = 0$ to $\xi = 1$ and decreases by 26% as τ increases with $\tau = 0$ to $\tau = 1$. However, the temperature $G(\xi, \eta, \tau)$ profile decrease about 35% and 40% as ξ increases from $\xi = 0$ to $\xi = 1$ and τ increases from $\tau = 0$ to $\tau = 1$, respectively.

The effects of mixed convection (buoyancy or Richardson number) parameter (Ri) and velocity ratio parameter (β) on velocity profiles $F(\xi, \eta, \tau)$ for accelerating flow $\phi(\tau) = 1 + \alpha\tau^2$, $\alpha = 0.5$ when *N* = 0.5, *Pr* = 0.7, Sc = 0.94, *Sr* = 0.5, *Df* = 0.5, $\mathrm{Re} = 2, \Gamma = 0.5, A = 1$ and $\xi = 0.5$ are depicted in Fig. 3. The magnitude of $F(\xi, \eta, \tau)$ increases with the increase of Ri. The velocity profile increases near the exponentially stretching surface and reduces when it moves away from the wall. Physically, assisting mixed convection parameter $(Ri > 0)$ acts like a favourable pressure gradient and the opposing mixed convection parameter $(Ri < 0)$ acts like an adverse pressure gradient which reduces the magnitude of the velocity significantly within the boundary layer for all the value $\beta = 0.5, 1.0, 1.5$. Further, for velocity ratio parameter $\beta < 1$ $(\beta = 0.5)$, the back flow is seen near the exponentially stretching surface due to $U_w > U_e$. When $\beta > 1$, the back flow is not much observed because $U_e > U_w$. In thermal and concentration profiles $(G(\xi, \eta, \tau), H(\xi, \eta, \tau))$ Ri is relatively less influenced and results are not plotted here to limit the number of graphs. Also, it is observed that for $\beta < 1$ $(\beta = 0.5)$, the magnitude of the back flow decreases in porous medium as compared with the case of fluid medium $(Da \to \infty)$ and for *Ri* = -2, -1 at $\beta \geq 1$, the magnitude of velocity decreases in porous medium as compared with fluid medium but the reverse trend is observed in *Ri* = 3 at $\beta = 1$. To be more specific, in particular, for accelerating flow $\phi(\tau) = 1 + \alpha\tau^2$, $\alpha = 0.5$ when *N* = 0.5, *Pr* = 0.7, Sc = 0.94, *Sr* = 0.5, *Df* = 0.5, $\mathrm{Re} = 2, \Gamma = 0.5, A = 1$ and $\xi = 0.5$ the velocity profile increases 22% and 25% as *Ri* increases from *Ri* = -1 to 1 and $\beta = 0.5$ *to* $\beta = 1.5$ in porous medium $(Da = 1)$ whereas the velocity profile increases 26% and 32% as *Ri* increases from *Ri* = -1 to 1 and $\beta = 0.5$ to $\beta = 1.5$ in case of fluid medium $(Da \to \infty)$.

The variations of the buoyancy (mixed convection) parameter (Ri) and Darcy number *Da* are presented in Fig. 4 for $\beta = 1.5$, $\Gamma = 0.5$, $N = 0.5$, $\mathrm{Re} = 2$, $\mathrm{Pr} = 0.7$, $Df = 0.5$, $Sr = 0.5$, $Sc = 0.94$ and $A = 1$. The skin friction coefficient $(\mathrm{Re})^{1/2} C_f$ increases with the increase of *Ri* $(Ri > 0)$, which acts like a assisting pressure gradient. $(\mathrm{Re})^{1/2} C_f$ increases in porous medium $(Da = 1)$ as compared with fluid medium $(Da \to \infty)$. In particular,

when $\beta = 1.5$, $\Gamma = 0.5$, $N = 0.5$, $\mathrm{Re} = 2$, $\mathrm{Pr} = 0.7$, $Df = 0.5$, $Sr = 0.5$, $Sc = 0.94$ and $A = 1$ at $\alpha = -0.2$,

IJARSE
ISSN (O) 2319 - 8354
ISSN (P) 2319 - 8346

$(\mathrm{Re})^{1/2} C_f$ increases approximately 111% and 161% as increase of *Ri* from $Ri = -1$ *to* 0 , in porous and fluid medium respectively.

Figures 5 and 6 illustrate the effects of N and Da on $F(\xi,\eta,\tau)$ and $(\mathrm{Re})^{1/2} C_f$ for $\alpha = 0.5$, *Pr* = 0.7, Sc = 0.94, *Sr* = 0.5, *Df* = 0.5, $\xi = 1.0$, *Ri* = 1, $\mathrm{Re} = 2$, $\beta = 1$, $\Gamma = 0.5$ and $A = 1$. It is clearly seen that Fig. 5 shows the velocity overshoot with increase of *N i. e.*, for aiding flow (*N*>0) and the magnitude of the overshoot decreases for negative values of *N i. e.*, for opposing flow (*N*<0). Further, the porous medium decreases the velocity overshoot as compared to the case of fluid medium. Also, suction reduces the momentum boundary layer thickness and avoid or delay the boundary layer separation. This will result in thin momentum boundary layer. The effects *Da* and N on $(\mathrm{Re})^{1/2} C_f$ are presented in Fig. 6. It is evident that the $(\mathrm{Re})^{1/2} C_f$ increases as N increases from -0.5 to 1. The physical reason is that *N* enhances the fluid acceleration and hence the $(\mathrm{Re})^{1/2} C_f$ increases. In particular, for instance, $\mathrm{Re} = 2$, $\beta = 1.0$, $Ri = 1, \mathrm{Pr} = 0.7, \beta = 1.5$, $\Gamma = 0.5, N = 0.5, \mathrm{Re} = 2$, $Df = 0.5, Sr = 0.5, Sc = 0.94$ and $A = 1$ at $\alpha = -0.2$, for accelerating flow $\phi(\tau) = 1 + \alpha\tau^2$, at $\alpha = 0.2$ for porous medium ($Da = 1$), $(\mathrm{Re})^{1/2} C_f$ increases about 89% with the increase of N from $N = 0$ to $N = 1$ while for fluid medium ($Da \to \infty$), $(\mathrm{Re})^{1/2} C_f$ increases about 87% when N increases from $N = 0$ to 1.

The effect of surface mass transfer A and velocity ratio parameter β on skin friction coefficient $(\mathrm{Re})^{1/2} Cf$ is graphically presented in Fig. 7 for accelerating flow $\phi(\tau) = 1 + \alpha\tau^2$, $\alpha = 0.2$ and decelerating flow $\phi(\tau) = 1 + \alpha\tau^2$, $\alpha = -0.2$ when *Ri* = 1, ξ = 1.0, Sc = 0.94, *N* = 0.5, $\mathrm{Re} = 2$, $\Gamma = 0.5$, $\mathrm{Pr} = 0.7$, $(\mathrm{Re})^{1/2} Cf$ Increases with increase of *A* (suction or A > 0) and decreases with *A* (injection or A < 0). In general suction enhances the skin friction whereas injection has the opposite tendency. Further, for $\beta < 1$, the fluid flows in opposite direction, because the wall velocity U_W is dominating over the free stream velocity U_e while for $\beta > 1$, the assisting flow is seen, the reason is that the free stream velocity U_e slowly dominating over the wall velocity U_W . Fig. 7 also shows that the $(\mathrm{Re})^{1/2} Cf$ raises for accelerating flow and suppresses for decelerating flow with velocity ratio parameter $\beta = 1.5$, but the reverse effect is observed with $\beta = 0.75$. In particular, for decelerating flow $\phi(\tau) = 1 + \alpha\tau^2$, $\alpha = -0.2$ when $N = 0.5$, $Ri = 1$, $\xi = 1$, $\mathrm{Re} = 2$, $\Gamma = 0.5$, $\mathrm{Pr} = 0.7$, $Sr = 0.5$, $Sc = 0.94, Df = 0.5, Da = 1$ at $\eta_\infty = 1.5$, $(\mathrm{Re})^{1/2} Cf$ increases 29% and 50% with the increase of *A* from *A* = -1 to 1 and β from $\beta = 0.75$ to $\beta = 1.5$, respectively.

IJARSE
ISSN (O) 2319 - 8354
ISSN (P) 2319 - 8346

The effects of Forchheimer's drag coefficient (Γ) and Darcy number (Da) on velocity profile $F(\xi,\eta,\tau)$ for accelerating flow

$\phi(\tau)=1+\alpha\tau^2$, $\alpha=1.0$ when $\mathrm{Re}=2$, $\beta=1.0$, $Ri=1$, $\mathrm{Pr}=0.7$, $Df=0.5, Sr=0.5, N=0.5$, $\xi=0.5, Sc=0.94, A=1$ are displayed in Fig. 8. It is observed that the magnitude of the velocity overshoot decreases with increase of Forchheimer's drag coefficient (Γ). Physically, the increase in inertial term implies that the porous medium is offering more resistant to the fluid flow. This results in the reduction of the velocity profile. The momentum boundary layer thickness reduces with the increase of drag coefficient (Γ). Thus, the non-Darcian term, *i.e.,* Forchheimer drag coefficient (Γ) has a very significant effect on the velocity distribution. Furthermore, the momentum boundary layer thickness reduces with increase of τ from 0 to 1.

The variations of the Dufour number *Df* and Prandtl number *Pr* on the temperature profile $G(\xi,\eta,\tau)$ are depicted in Fig. 9 for α = 0.5,*Ri* =1,ξ =0.5 ,Sc = 0.66,*N*= 0.5, $\mathrm{Re}=2$ and $\Gamma=0.5, \beta=0.5, Sr=0.3, Da=1, A=1.$ The profile $G(\xi,\eta,\tau)$ increases remarkably within the thermal boundary layer when Df is increased from Df = 0.1 to Df = 1.0 as observed in Fig. 9. The reason is that the Dufour term which appears in temperature equation measures the concentration gradient to energy flux in the flow domain. It has significant role in enhancing the energy in the boundary layer. Further, $G(\xi,\eta,\tau)$ decreases as the *Pr* increases from 0.7 to 7.0. It is worthy to mention that higher values of *Pr* (*Pr* =7.0) means the more viscous fluid and have low thermal conductivity which reduce the thermal boundary layer thickness. Also, the magnitude of profile $G(\xi,\eta,\tau)$ decreases significantly with the increase of τ from 0 to 1. In particular, for accelerating flow $\phi(\tau)=1+\alpha\tau^2$, $\alpha=0.5$ when $\Gamma=0.5$, *Pr* = 7.0, *Ri* = 1, ξ = 0.5, Sc = 0.66, $\beta=0.5, \mathrm{Re}=2$, $Sr=0.5$ Df =0.3, A=1 and *N* = 0.5, $G(\xi,\eta,\tau)$ increases approximately by 92% for the increase in *Df* from 0.5 to 1.0 in both cases of porous (Da=1) and fluid medium ($Da\to\infty$) in unsteady case ($\tau>0$).

The effects of *Df* and *Da* on heat transfer coefficient is presented in Fig. 10 for *Ri* =1, ξ = 1.0, Sc = 0.94, *N* = 1.0, $\mathrm{Re}=2$, $\mathrm{Pr}=0.7$, $\Gamma=0.5$, $\beta=0.5$, $Sr=0.5$ and $A=1.$ The heat transfer coefficient $(\mathrm{Re})^{-1/2}Nu$ decreases with the increase of *Df* from *Df* = 0.1 to 1.0. Further, $(\mathrm{Re})^{-1/2}Nu$ increases in case of fluid medium $(Da\to\infty)$ as compared with porous medium $(Da=1)$. In particular, for decelerating flow $\phi(\tau)=1+\alpha\tau^2$, $\alpha=-0.2$ when *Ri* =1,ξ = 1.0, Sc = 0.94, *N* = 1.0, *Pr* = 0.7, $\mathrm{Re}=2$, $\Gamma=0.5$, $\beta=0.5$, $Sr=0.5$ and $A=1$,

$(\mathrm{Re})^{-1/2}Nu$ increases33% and 44% in with porous medium and fluid medium, respectively.

IJARSE
ISSN (O) 2319 - 8354
ISSN (P) 2319 - 8346

Figure 11 illustrates the influence of Soret number *Sr* and Schmidt number *Sc* for accelerating flow $\phi(\tau)=1+\alpha\tau^2,\ \alpha=0.5$ with $N=0.5,\ Ri=1.0,\ \xi=0.5,\ \Pr=0.7,\ \Gamma=0.3,\ \beta=1.5,\ Df=0.3,\ Da=1.$ It is observed that the increase in *Sr* from 0.5 to 1.0 increases the concentration profile. Physically, the reason is that the *Sr* appears in concentration equation which measures temperature gradient to mass flux. Also, increase in Sc decreases the concentration profile $H(\xi,\eta,\tau)$. It is due to the fact that increase in *Sc* means decrease of diffusivity that result in decrease of concentration boundary layer. Thus, the concentration of species is high for small values of *Sc* and low for high values of *Sc*. Further, suction (*A*> 0) decreases the concentration boundary layer thickness while injection (*A*< 0) has reverse effect. In particular, for instance for accelerating flow $\phi(\tau)=1+\alpha\tau^2,\ \alpha=0.5$ when *Ri* =1,ξ =0.5 ,*N*= 0.5, $\mathrm{Re}=2$, $\Gamma=0.3, \beta=1.5, Df=0.3, Da=1$ at A = 1.0 the concentration profile decreases 51% and 36% with the increase of Sc from 0.22 to 2.57 , and with the increase of *Sr* for 0.5 to 1.0, respectively.

Figure 12 displays the effects of *Sr* and *Sc* on $H(\xi,\eta,\tau)$ for accelerating flow $\phi(\tau)=1+\alpha\tau^2,\ \alpha=0.5$ when *Ri* =1,ξ = 0.5, Pr = 0.7, *N*= 0.5, *Df* = 0.3, $\mathrm{Re}=2,\ \Gamma=0.5, \beta=0.5, Da=1$ and $A=1.$ It is observed from Fig. 12 that the increase of the *Sr* increases the concentration profile $H(\xi,\eta,\tau)$. This is because of the reason of combined effects of matter and thermal diffusion with cross diffusion (Soret and Dufour) effects. Here, the realistic values of Schmidt number Sc = 0.94 and 2.57, representing the diffusion of species of most common interest such as water vapour and Propyl benzene etc. at 25^0 C at one atmospheric pressure. Also increase of *Sc* decreases the concentration profile $H(\xi,\eta,\tau)$. Physically, the higher values of Schmidt number have a low mass diffusivity which results to decrease in the thickness of the concentration boundary layer. In temperature and velocity profiles effect of *Sc* is negligibly small because *Sc* parameter appears only in the concentration equation. Thus, the effect of *Sc* on those profiles is not presented here. Further, increase in τ from 0 to 1 result into thin concentration boundary layer and species concentration profile decreases within the concentration boundary layer.

Figure 13 illustrates the effects of *Sr* and *Da* on Sherwood number (mass transfer coefficient) $(\mathrm{Re})^{-1/2}Sh$ for accelerating flow $\phi(\tau)=1+\alpha\tau^2,\ \alpha>0$ and decelerating flow $\phi(\tau)=1+\alpha\tau^2,\ \alpha<0$ when *Ri* =1,ξ = 1.0, *Df* = 0.5, Sc = 0.94, *N*= 1.0, *Pr* = 0.7, $\mathrm{Re}=2,\ \Gamma=0.5,\ \beta=0.5\ and\ A=1.$ Fig. 13 shows that the increase of the *Sr* decreases $(\mathrm{Re})^{-1/2}Sh$. Moreover, $(\mathrm{Re})^{-1/2}Sh$ decreases in both the cases of porous and fluid medium ($Da=1.0$ and $Da\to\infty$) respectively. In particular, for example in decelerating flow at $\alpha=-0.2$ with *N*= 1.0, *Ri* = 1, ξ = 1.0, *Df* = 0.5, *Pr* = 0.7, *Sc* = 0.94, $\mathrm{Re}=2, \Gamma=0.5, \beta=0.5$ and $A=1$, Sherwood number decreases 28% with the increase of *Sr* from 0.5 to 1.0 and same effect will observed in porous and fluid medium.

International Journal of Advance Research in Science and Engineering
Vol. No.5, Issue No. 10 , October 2016
www.ijarse.com
IJARSE
ISSN (O) 2319 - 8354
ISSN (P) 2319 - 8346

V. CONCLUSIONS

The present analysis is carried out for the unsteady mixed convection flow over permeable exponentially stretching surface through Darcy-Forchheimerporous medium in presence of cross diffusion (Dufour and Soret) effects. The resulting system of dimensionless coupled nonlinear partial differential equation was solved by using an implicit finite difference scheme in combination with Quasi-linearization technique. From this numerical investigation the following conclusions are drawn.

- The magnitude of velocity and temperature profiles decrease for the increase in the streamwise coordinate ξ and time τ . In particular,

  When $\alpha = 1,\ \mathrm{Re} = 2,\ \beta = 0.5,\ Ri = 1,\ \mathrm{Pr} = 0.7,$

  $Df = 0.5, Sr = 0.5, \Gamma = 0.5, N = 1, A = 1, Da = 1,$ the velocity profile and temperature profile decreases by 11% and 35% as ξ increases from $\xi = 0$ to $\xi = 1$ for $\tau = 0$.
- The mixed convection parameter enhances the skin friction coefficient in accelerating flow and reduces the friction in decelerating flow. For instance, in decelerating flow $\phi(\tau) = 1 + \alpha\tau^2,\ \alpha = -0.2$ when *N* = 0.5, *Pr* = 0.7, Sc = 0.94, *Sr* = 0.5, *Df* = 0.5, $\mathrm{Re} = 2, \Gamma = 0.5, A = 1$ and $\xi = 1.0$ the $(\mathrm{Re})^{1/2} Cf$ decreases 69% and 76% as *Ri* increases from *Ri* = -1 to 1 with porous medium $(Da = 1)$ and fluid medium $(Da \to \infty)$, respectively
- The thickness of the thermal boundary layer increases with the increase of *Df* and decreases with the increase of *Pr* because higher Prandtl number have low thermal conductivity. For example, for accelerating flow $\phi(\tau) = 1 + \alpha\tau^2,\ \alpha = 0.5$ when $\Gamma = 0.5$, *Pr* = 0.7, *Ri* = 1,ξ =0.5, Sc = 0.66, $\beta = 0.5, \mathrm{Re} = 2$, $Sr = 0.5$ $Df = 0.3, A = 1$ and *N* = 0.5, temperature profile increases approximately by 20% and 22% for the increase in *Df* from 0.5 to 1.0 in both cases of porous ($Da = 1$) and fluid medium ($Da \to \infty$) in unsteady case ($\tau > 0$).
- An increase in the Dufour number (*Df*) decreases the Nusselt number (*Nu*). In particular, for instance when*Pr* = 0.7, *Ri* =2,ξ =1.0,Sc = 0.94, $\mathrm{Re} = 10,\ Sr = 0.5$ and *N* = 0.5 $(\mathrm{Re})^{-1/2} Nu$ decreases approximately by 56% and 55% with the increase of *Df* from 0.1 to 1.0 with porous medium and fluid medium, respectively.
- The Concentration boundary layer thickness increases with increase in the Soret number *Sr* and decreases with the increase in Schmidt number Sc. In particular, for example, in accelerating flow $\alpha = 0.5$ with *Pr* = 0.7, *Ri* = 1, ξ = 0.5, *N* = 0.5, *Df* = 0.5, $\mathrm{Re} = 2, \Gamma = 0.5, \beta = 0.5$ and $A = 1$ at Sc = 2.57 the concentration profile increases 68% and 74% with the increase of *Sr* from 0.5 to 1.0 and time τ from 0 to 1.

IJARSE
ISSN (O) 2319 - 8354
ISSN (P) 2319 - 8346

VI. ACKNOWLEDGEMENTS

Dr. P. M. Patil acknowledges the support by the Major Research Project with ID: MRP-MAJOR-MATH-2013-6619 and F. No. 43-413/2014(SR) dated 30th October 2015 funded by the University Grants Commission, New Delhi – 110 002, India. Nafisa A. Kumbarwadi expresses her sincere thanks to the UGC New Dehli-110 002 for award of Maulana Azad National Fellowship. E. Momoniat thanks the National Research Foundation of South Africa under grant number 103483 for their support.

Table 1. Values of $\left[-g_{\eta}(0)\right]$ for varius values of Prandtl number *Pr* with *Re* = 2, $\alpha = 0,\ Df = 0,$ and *N* = 0, $Da = 1,\ Sr = 0,\ Ri = 0$.

Pr	**0.7**	**1.0**	**2.0**	**7.0**	**10.0**	**100**
Patil[12]	0.354215	0.444428	0.683024	1.386861	1.680150	5.547512
Patil et al.[13]	0.352215	0.444428	0.683024	1.386861	1.680150	5.547512
Ravindran and Samyuktha[9]	0.354200	0.444500	0.683000	1.386900	1.680200	5.547500
Present work	0.351270	0.444510	0.683300	1.386900	1.680300	5.547520

Table. 2: Values of $(\mathrm{Re})^{1/2} C_f$, $(\mathrm{Re})^{-1/2} Nu$, $(\mathrm{Re})^{-1/2} Sh$ for different values of Prandtl number *Pr* with $\alpha = 0.2, \xi = 1, \mathrm{Re} = 2.$

Pr	*Ri*	β	*N*	Γ	*Da*	*Df*	*Sr*	Sc	*A*	τ	$(\mathrm{Re})^{1/2} C_f$	$(\mathrm{Re})^{-1/2} Nu$	$(\mathrm{Re})^{-1/2} Sh$
0.7	1.0	1.0	-0.5	0.5	1	0.5	0.5	0.94	1	1	0.19593	2.50555	3025855
0.7	1.0	1.0	-0.5	0.5	1	0.5	0.5	0.94	1	1.5	0.16560	2.95387	3.80505
0.7	1.0	1.0	-0.5	0.5	1	0.5	0.5	0.94	1	2	0.13665	3.50791	4.47841
0.7	1.0	1.5	-0.5	0.5	1	0.5	0.5	0.94	1	1	3.68332	2.79213	3.56612
0.7	1.0	1.5	-0.5	0.5	1	0.5	0.5	0.94	1	1.5	6.23130	3.31497	4.19480
0.7	1.0	1.5	-0.5	0.5	1	0.5	0.5	0.94	1	2	10.45895	3.94758	4.95465
0.7	1.0	1.0	1.0	0.5	1	0.5	0.5	0.94	1	1	0.67207	2.53840	3.29612
0.7	1.0	1.0	1.0	0.5	1	0.5	0.5	0.94	1	1.5	0.57200	2.97412	3.82833
0.7	1.0	1.0	1.0	0.5	1	0.5	0.5	0.94	1	2	0.47516	3.51898	4.49089
0.7	1.0	1.0	1.0	0.5	∞	0.5	0.5	0.94	1	1	0.70869	2.54243	3.30059
0.7	1.0	1.0	1.0	0.5	∞	0.5	0.5	0.94	1	1.5	0.59768	2.97648	3.83072
0.7	1.0	1.0	1.0	0.5	∞	0.5	0.5	0.94	1	2	0.49120	3.51984	4.49196
7.0	1.0	1.0	1.0	0.5	1	0.3	0.3	0.94	1	1	0.42463	15.56929	2.60238
7.0	1.0	1.0	1.0	0.5	1	0.3	0.3	0.94	1	1.5	0.36256	17.16324	3.12491
7.0	1.0	1.0	1.0	0.5	1	0.3	0.3	0.94	1	2	0.30382	19.10971	3.77216
7.0	1.0	1.0	1.0	0.5	∞	0.3	0.3	0.94	1	1	0.44210	15.57136	2.60482

7.0	1.0	1.0	1.0	0.5	∞	0.3	0.3	0.94	1	1.5	0.37461	17.16457	3.12634
7.0	1.0	1.0	1.0	0.5	∞	0.3	0.3	0.94	1	2	0.31118	19.11007	3.77275
7.0	1.0	1.5	1.0	0.5	1	0.3	0.3	0.94	1	1	3.89278	15.92869	2.92605
7.0	1.0	1.5	1.0	0.5	1	0.3	0.3	0.94	1	1.5	6.40927	17.65357	3.53596
7.0	1.0	1.5	1.0	0.5	1	0.3	0.3	0.94	1	2	10.60902	19.74131	4.27352

Nomenclature

L characteristic length (m)

g acceleration due to gravity (ms^{-2})

x, y Cartesian coordinates (m)

u velocity component in the x direction ($m\ s^{-1}$)

v velocity component in the y direction($m\ s^{-1}$)

f dimensionless stream function

C species concentration ($kg\ m^{-3}$)

C_f local skin-friction coefficient

C_p specific heat at constant pressure ($J\ K^{-1}kg^{-1}$)

C_s the concentration susceptibility

C_w concentration at the wall ($kg\ m^{-3}$)

C_{w0} reference concentration

C_∞ ambient species concentration

Df Dufour number

Da Darcy number

F dimensionless velocity

G dimensionless temperature

Gr, Gr^* Grashof numbers due to temperature and species concentration, respectively

H dimensionless species concentration

N ratio of buoyancy forces

Nu Nusselt number

$\Pr$ Prandtl number (ν/α)

Re Reynolds number

Ri Richardson number

IJARSE
ISSN (O) 2319 - 8354
ISSN (P) 2319 - 8346

S Empirical constant in the second-order resistant term

Sc Schmidt number (ν/D_m)

Sr Soret number

t time

T temperature (K)

T_m the mean fluid temperature (K)

T_w temperature at the wall (K)

T_{w0} reference temperature

T_∞ ambient temperature (K)

Greek symbols

α thermal diffusivity ($m^2 s^{-1}$)

β, β^* volumetric coefficients of the thermal and concentration expansions, respectively (K^{-1})

ξ, η, τ transformed variables

μ dynamic viscosity (kg $m^{-1} s^{-1}$)

ν kinematic viscosity ($m^2 s^{-1}$)

$\phi(\tau)$ unsteady function of τ

ρ density (kg m^{-3})

ψ streamfunction

Γ Forchheimer's drag parameter

Subscripts

w condition at the wall

e free stream condition

ξ, η, τ denote the partial derivatives with respect to these variables, respectively.

REFERENCES

[1] G. H. R. Kefayati., The simulation of double-diffusive natural convection and entropy generation of power law fluids in an inclined porous cavity with Soret and Dufour effects (Part I: Study of fluid flow, heat and mass transfer), Int. J. Heat Mass Transfer, 94(2016)539-581.

[2] D. Srinivasacharya, B. Mallikarjuna, R. Bhuvanavijay., Soret and Dufour effects on mixed convection along a vertical wavy surface in a porous medium with variable properties, Ain. Shams Engg, 6(2015)553-564.

[3] P. M. Patil, S. Roy, E. Momoniat., Thermal diffusion and diffusion-thermo effects on mixed convection from an exponentially impermeable stretching surface, Int. J. Heat Mass Transfer, 100(2016)482-489.

IJARSE
ISSN (O) 2319 - 8354
ISSN (P) 2319 - 8346

[4] Chein-Hsinn Chen, Cha'o-kuangChen., Non-Darcian mixed convection along a vertical plate embedded in a porous medium, Appl. Math. Modelling, 14(1990)482-488.

[5] D. Pal, H. Mondal., Effect of variable viscosity on MHD non-Darcy mixed convective heat transfer over a stretching sheet embedded in a porous medium with non-uniform heat source/sink, Comm. Nonlinear. Sci. Numer. Simulat, 15(2010)1553-1564.

[6] M. K. Partha, P. V. S. N. Murthy, G. P. Rajasekhar., Soret and Dufour effects in a non-Darcy porous medium, J. Heat Transfer,108(2006)605-610.

[7] A. J. Chamkha, A. M. Aly, M. A. Mansour., Similarity solution for unsteady heat and mass transfer from a stretching surface embedded in a porous medium with suction/injection and chemical reaction effects, Chem. Eng. Comm. 197(2010)846-858.

[8] S. Mukhopadhyay., Slip effects on MHD boundary layer flow over an exponentially stretching sheet with suction/blowing and thermal radiation, Ain Shams Engg. Journal, 4(2013)485-491.

[9] R. Ravindran, N. Samyuktha., Unsteady mixed convection flow over stretching sheet in presence of chemical reaction and generation or absorption with non-uniform slot suction or injection, App. Math. Mech. Engl. Ed, 36(2015)1253-1272.

[10] I. Mandal, S. Mukhopadhyay., Heat transfer analysis for fluid flow over an exponentially stretching porous sheet with surface heat flux in porous medium, Ain. Shams Engg, 4(2013)103-110.

[11] K. Sharada. Bhandari. S., MHD mixed convection flow of a Casson fluid over an exponentially stretching surface with the effects of Soret, Dufour, thermal radiation and chemical reaction, World J. Mech, 5(2015)165-177.

[12] P. M. Patil, Effects of surface mass transfer on steady mixed convection flow from vertical stretching sheet with variable wall temperature and concentration., Int. J. Num. Heat Fluid Flow,22(2012)287-305.

[13] P. M. Patil, I. Pop and S. Roy., Unsteady heat and mass transfer over a vertical stretching sheet in a parallel free stream with variable wall temperature and concentration, Num. Meth. Partial Diff.Equa, 28(2012)929-941.

[14] K. Inouye, A. Tate., Finite difference version Quasi-linearization applied to boundary layer equations, AIAA J, **12** (1976) 558- 560.

[15] H. Schlichting, K. Gersten., Boundary Layer Theory, Springer, New York (2000).

[16] P. M. Patil, A. J. Chamkha., Heat and mass transfer from mixed convection flow of polar fluid along a plate in porous medium with chemical reaction, Int. J. Num. Meth. Heat and Fluid Flow,23(2013)899-926.

[17] R. S. Varga., Matrix Iterative Analysis, Prentice Hall (2000).

International Journal of Advance Research in Science and Engineering
Vol. No.5, Issue No. 10 , October 2016
www.ijarse.com
IJARSE
ISSN (O) 2319 - 8354
ISSN (P) 2319 - 8346

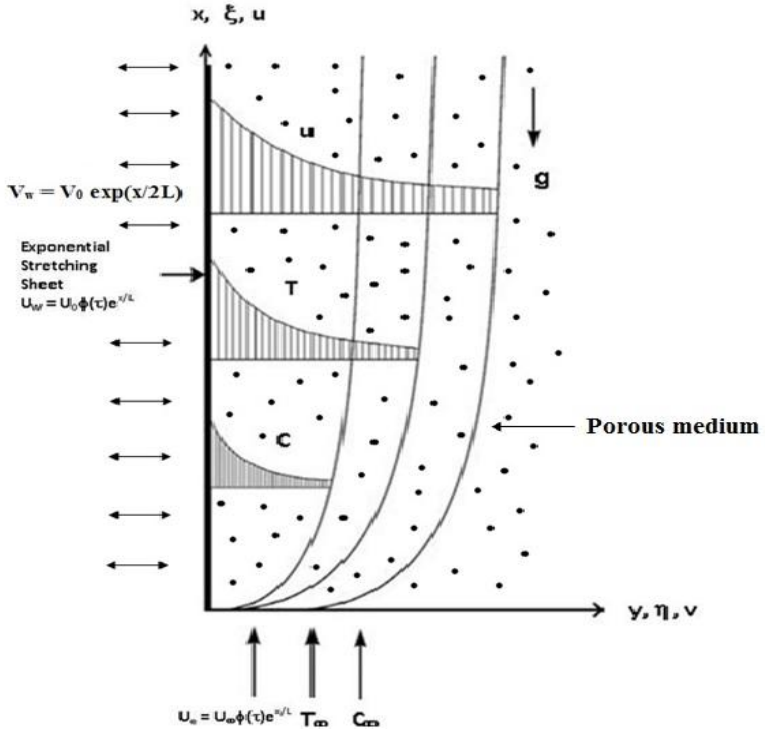

Fig. 1.The physical model and coordinate system

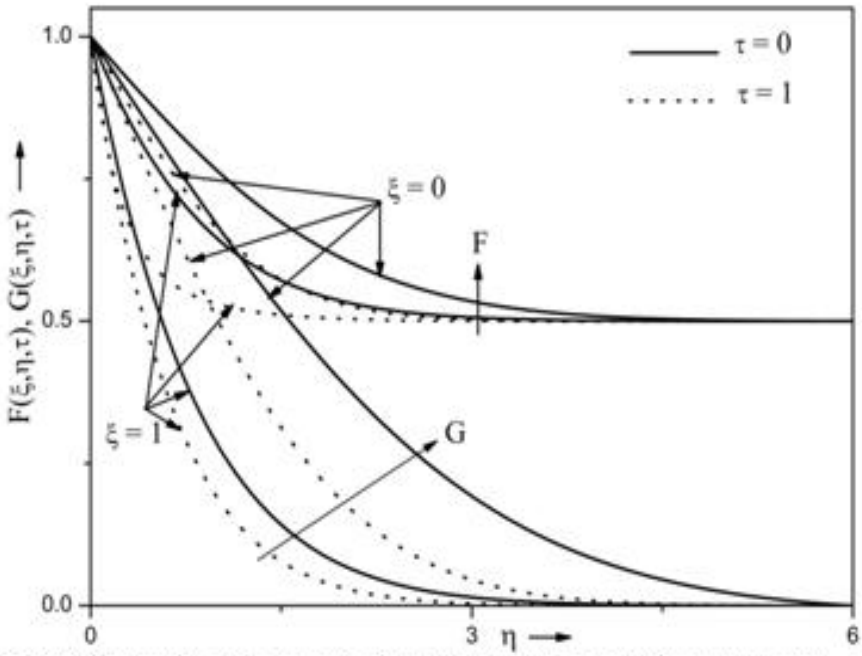

Fig 2: Effects of ξ and τ on velocity and temperature profile where $\phi(\tau) = 1+\alpha\tau^2$ for $\alpha = 1.0$, $Ri = 1.0$, $\beta = 0.5$, $\Gamma = 1.0$, $Re = 2.0$, $Pr = 0.7$, $Df = 0.5$, $Sr = 0.5$, $Sc = 0.94$, $Da = 1.0$ and $A = 1$.

International Journal of Advance Research in Science and Engineering
Vol. No.5, Issue No. 10 , October 2016
www.ijarse.com
IJARSE
ISSN (O) 2319 - 8354
ISSN (P) 2319 - 8346

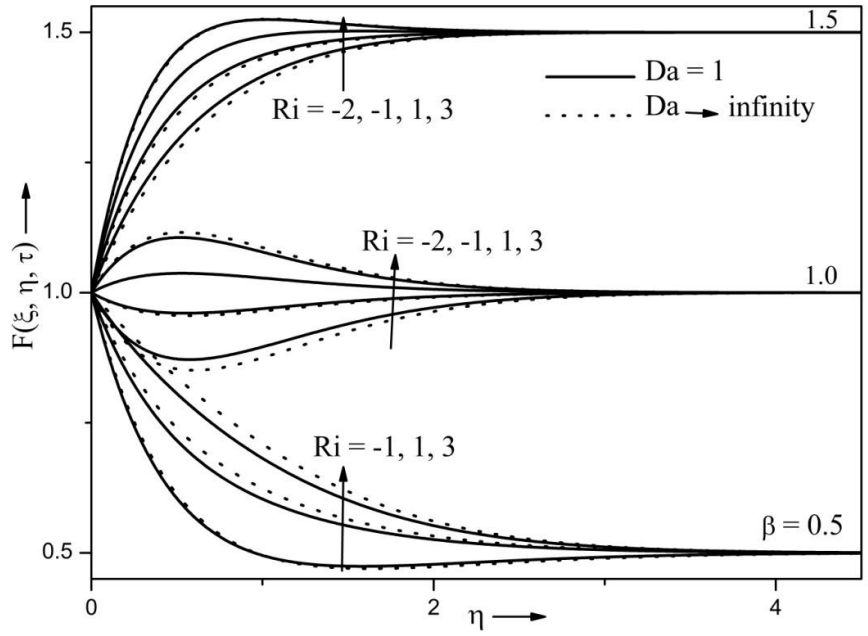

Fig 3: Effects of *Ri* and *Da* on velocity profile where $\phi(\tau) = 1+\alpha\tau^2$ for $\alpha = 0.5$, $\Gamma = 0.5$, $N = 0.5$, $Re = 2.0$, $Pr = 0.7$, $Df = 0.5$, $Sr = 0.5$, $Sc = 0.94$ and $A = 1.0$.

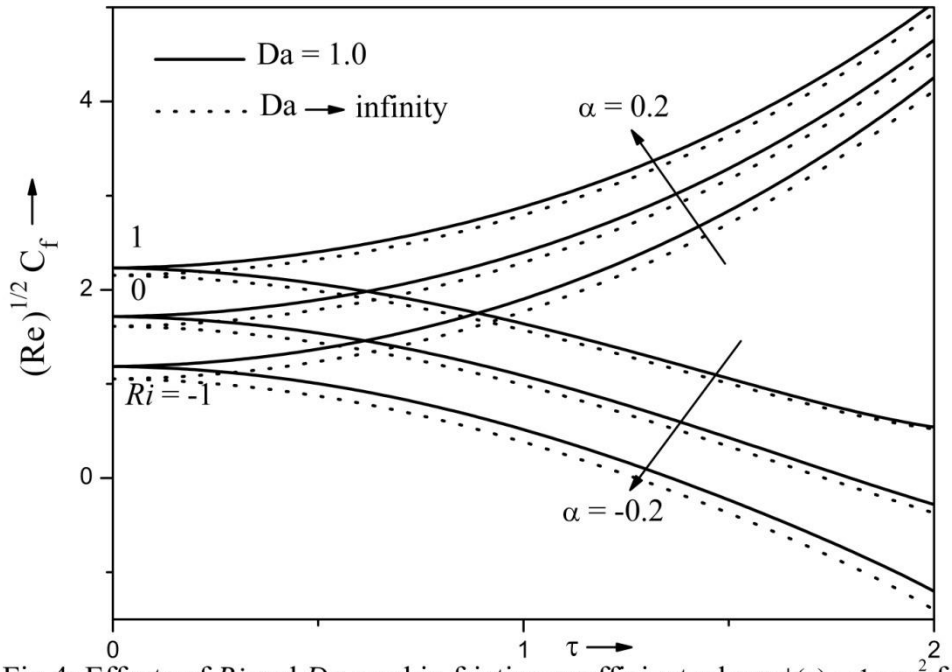

Fig 4: Effects of *Ri* and *Da* on skin friction coefficient where $\phi(\tau) = 1+\alpha\tau^2$ for $\beta = 1.5$, $\Gamma = 0.5$, $N = 0.5$, $Re = 2.0$, $Pr = 0.7$, $Df = 0.5$, $Sr = 0.5$, $Sc = 0.94$ and $A = 1.0$.

International Journal of Advance Research in Science and Engineering
Vol. No.5, Issue No. 10 , October 2016
www.ijarse.com
IJARSE
ISSN (O) 2319 - 8354
ISSN (P) 2319 - 8346

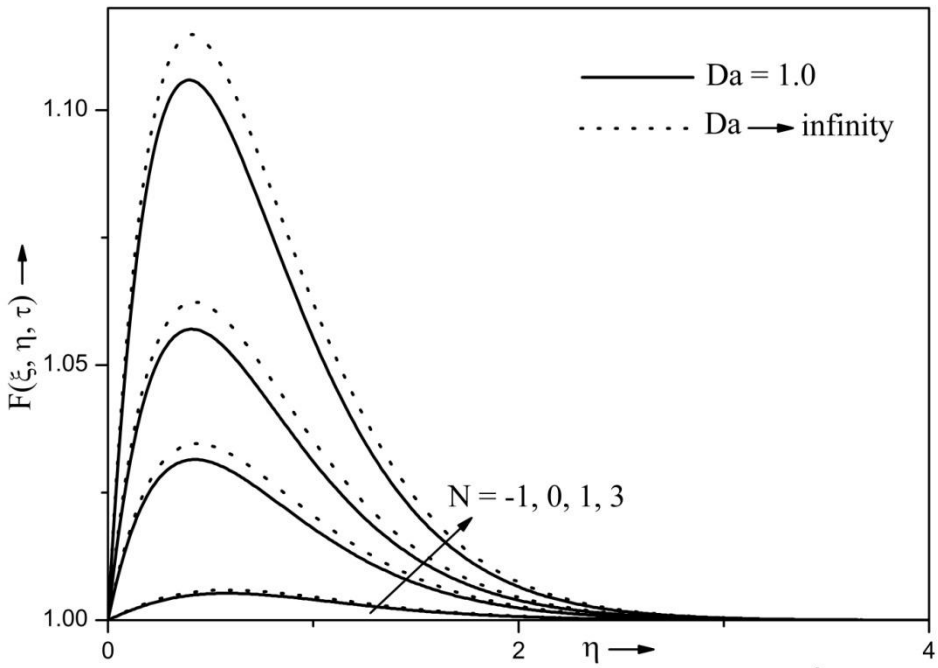

Fig 5: Effects of N and Da on velocity profile where $\phi(\tau) = 1+\alpha\tau^2$ for $\alpha = 0.5$, $\xi = 1.0$, $Ri = 1.0$, $\beta = 1.0$, $\Gamma = 0.5$, $Re = 2.0$, $Pr = 0.7$, $Df = 0.5$, $Sr = 0.5$, $Sc = 0.94$ and $A = 1$.

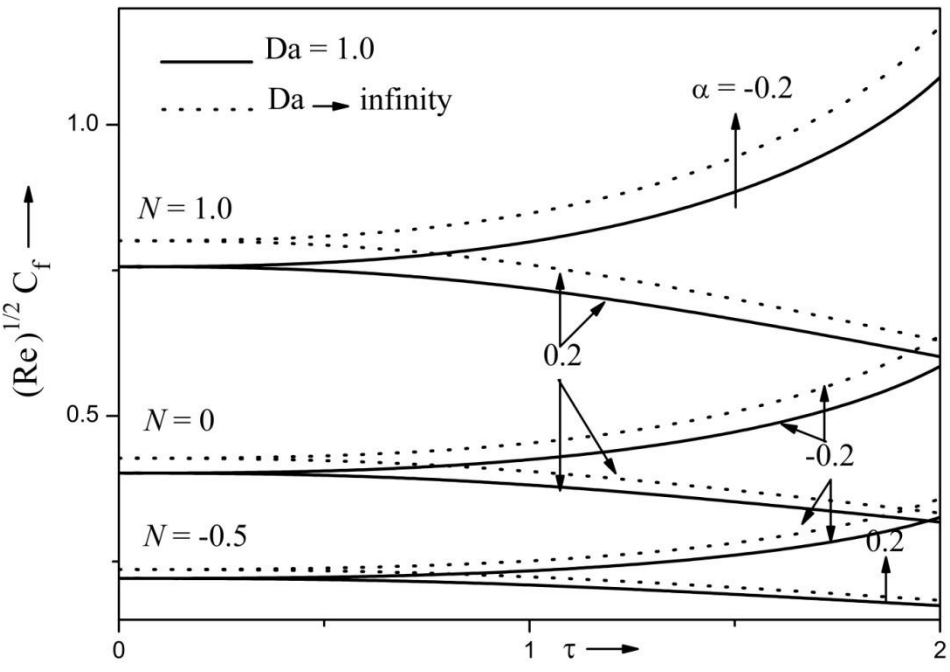

Fig 6: Effects of N and Da on skin friction coefficient where $\phi(\tau) = 1+\alpha\tau^2$ for $Ri = 1.0$, $\Gamma = 0.5$, $Re = 2.0$, $Pr = 0.7$, $Df = 0.5$, $Sr = 0.5$, $Sc = 0.94$ and $A = 1$.

International Journal of Advance Research in Science and Engineering
Vol. No.5, Issue No. 10 , October 2016
www.ijarse.com
IJARSE
ISSN (O) 2319 - 8354
ISSN (P) 2319 - 8346

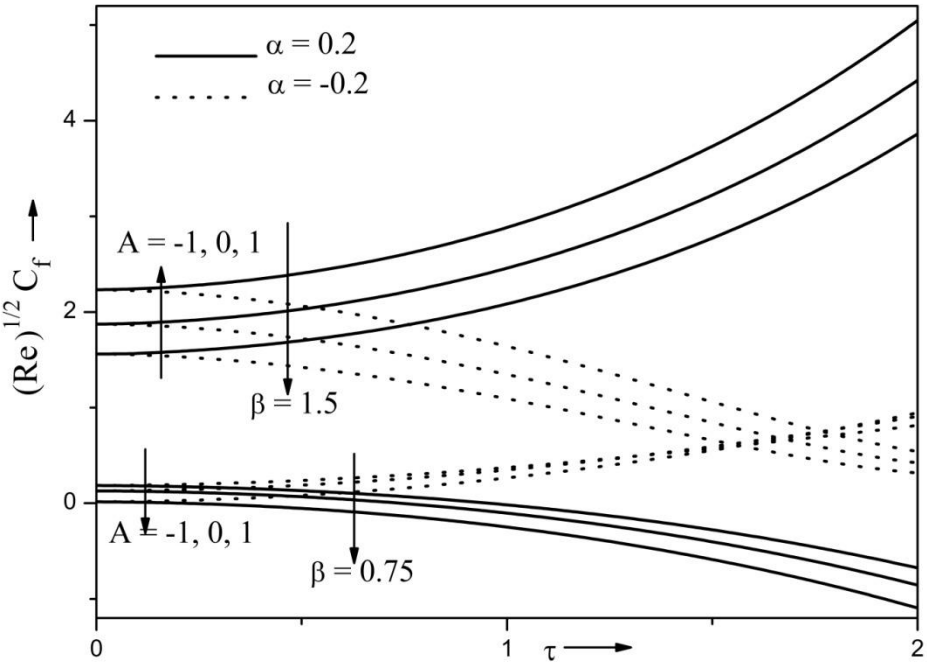

Fig 7: Effects of A and β on skin friction coefficient where $\phi(\tau) = 1+\alpha\tau^2$ for $Ri = 1.0$ $\Gamma = 0.5$, $N = 0.5$, $Re = 2.0$, $Pr = 0.7$, $Df = 0.5$, $Sr = 0.5$, $Sc = 0.94$ and $Da = 1.0$.

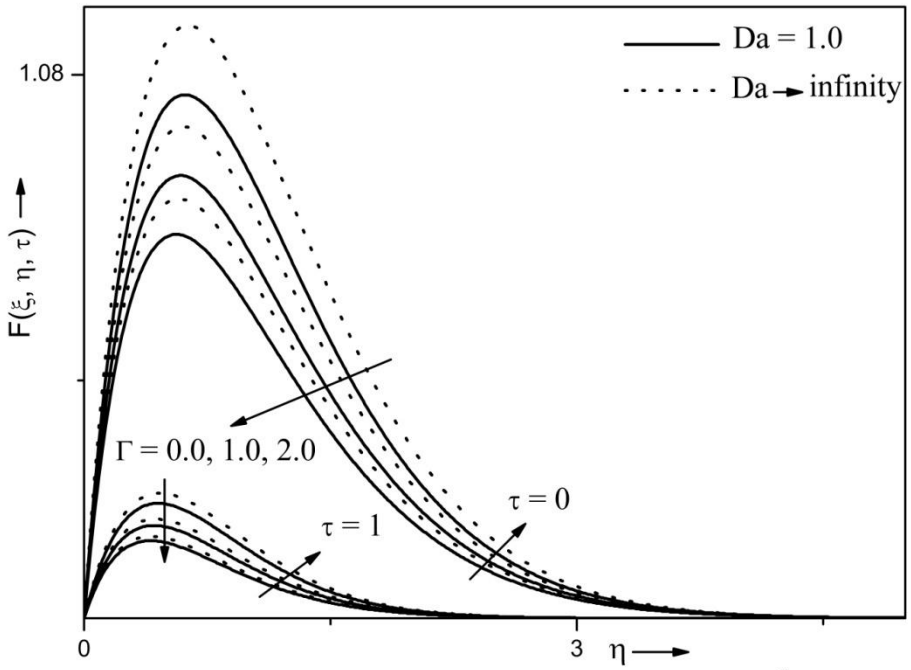

Fig 8: Effects of Γ and Da on velocity profile where $\phi(\tau) = 1+\alpha\tau^2$ for $\alpha = 1.0$, $\xi = 0.5$, $\beta = 1.0$, $N = 0.5$, $Ri = 1.0$, $Re = 2.0$, $Pr = 0.7$, $Df = 0.5$, $Sr = 0.5$, $Sc = 0.94$ and $A = 1$.

International Journal of Advance Research in Science and Engineering
Vol. No.5, Issue No. 10 , October 2016
www.ijarse.com
IJARSE
ISSN (O) 2319 - 8354
ISSN (P) 2319 - 8346

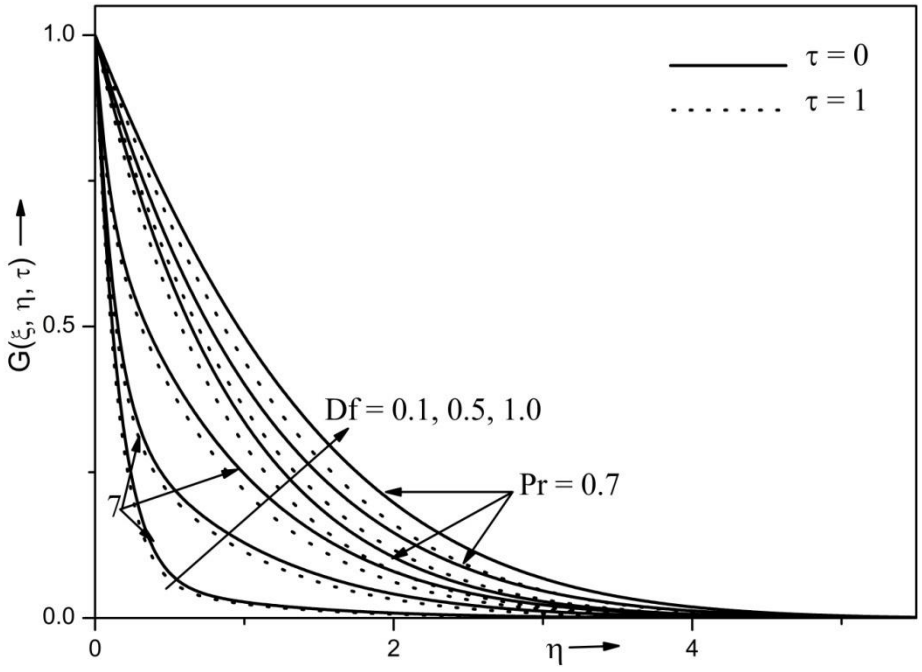

Fig 9: Effects of *Df* and *Pr* on temperature profile where $\phi(\tau) = 1+\alpha\tau^2$ for $\alpha = 0.5$, $\beta = 0.5$, $\Gamma = 0.5$, $N = 0.5$, $Re = 2.0$, $Sr = 0.3$, $Sc = 0.66$ $Ri = 1.0$, $Da = 1$ and $A = 1.0$.

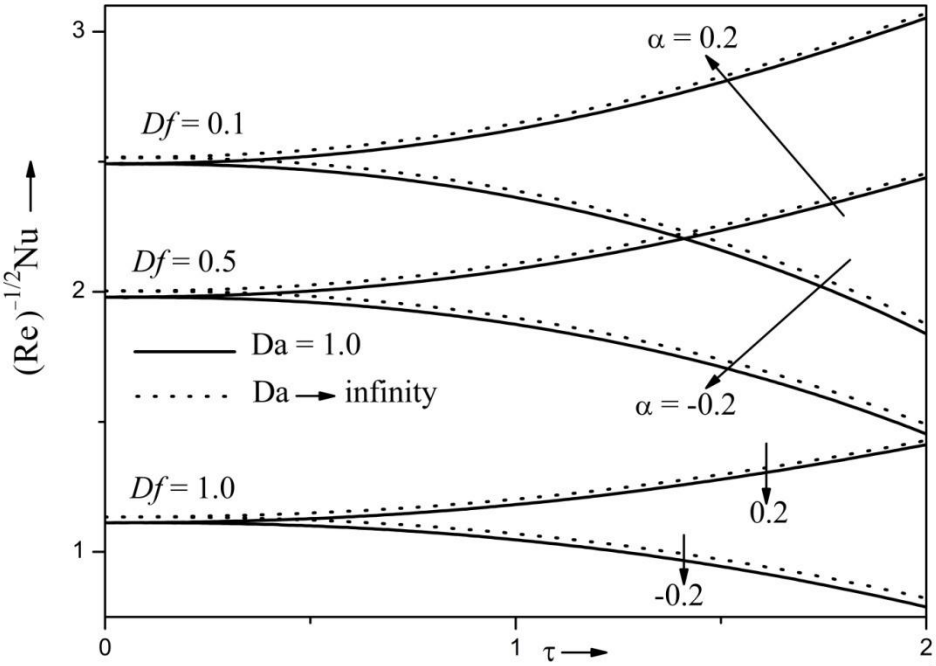

Fig 10: Effects of *Df* and *Da* on heat transfer coefficient where $\phi(\tau) = 1+\alpha\tau^2$ for $\beta = 0.5$, $\Gamma = 0.5$, $N = 1.0$, $Ri = 1.0$, $Re = 2.0$, $Pr = 0.7$, $Sr = 0.5$, $Sc = 0.94$ and $A = 1.0$.

IJARSE
ISSN (O) 2319 - 8354
ISSN (P) 2319 - 8346

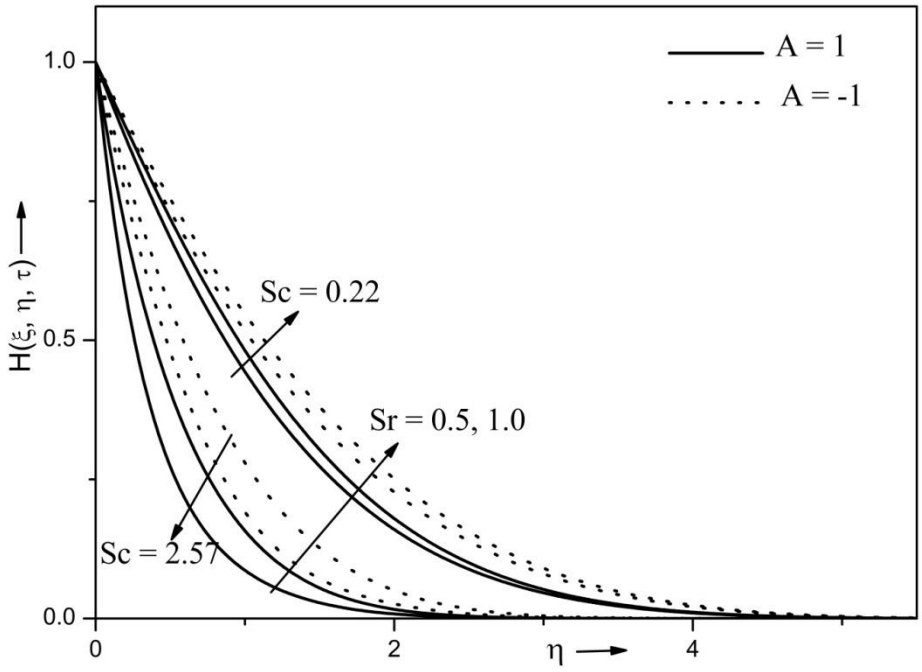

Fig 11: Effects of *Sr* and *Sc* on concentration profile where $\phi(\tau) = 1+\alpha\tau^2$ for $\alpha = 0.5$, $\beta = 1.0$, $\Gamma = 0.3$, $N = 0.5$, $Ri = 1.0$, $Re = 2.0$, $Pr = 0.7$, $Df = 0.3$, $Da = 1$.

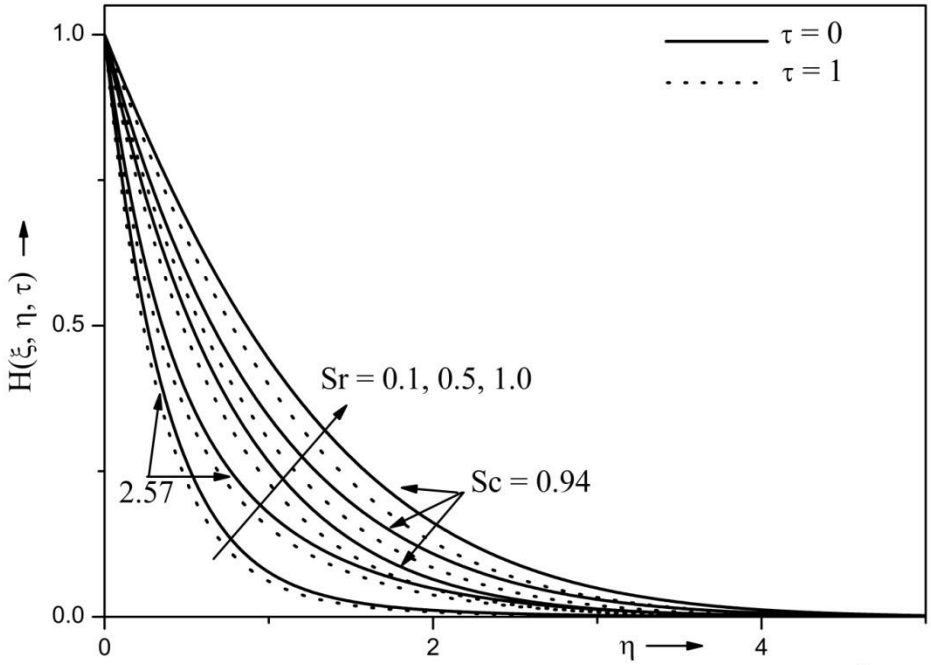

Fig 12: Effects of *Sr* and *Sc* on concentration profile where $\phi(\tau) = 1+\alpha\tau^2$ for $\alpha = 0.5$, $\beta = 0.5$, $\Gamma = 0.5$, $N = 0.5$, $Ri = 1.0$, $Re = 2.0$, $Pr = 0.7$, $Df = 0.5$, $Da = 1$ and $A = 1.0$.

International Journal of Advance Research in Science and Engineering
Vol. No.5, Issue No. 10 , October 2016
www.ijarse.com
IJARSE
ISSN (O) 2319 - 8354
ISSN (P) 2319 - 8346

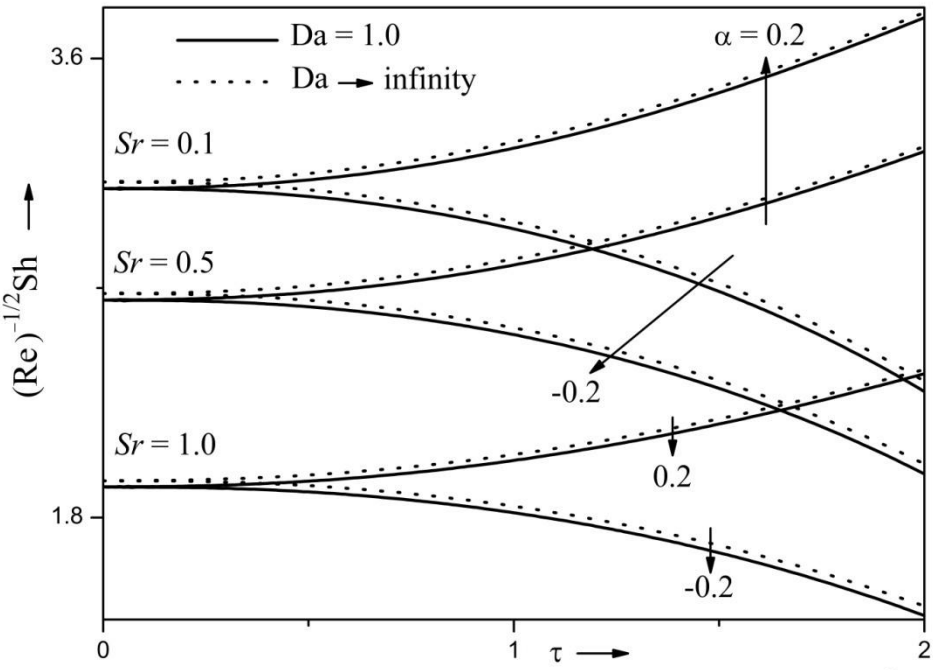

Fig 13: Effects of *Sr* and *Da* on mass transfer coefficient where $\phi(\tau) = 1+\alpha\tau^2$ for $\beta = 0.5$, $\Gamma = 0.5$, $N = 1.0$, $Ri = 1.0$, $Re = 2.0$, $Pr = 0.7$, $Df = 0.5$, $Sc = 0.94$ and $A = 1.0$.